Supporting Information

Vacuum Vapor Migration Strategy for Atom-Nanoparticle Composite Catalysts Boosting Bifunctional Oxygen Catalysis and Rechargeable Zn-Air Batteries

Yun-Long Zhang, Yun-Kun Dai, Bo Liu, Xiao-Fei Gong, Lei Zhao*, Feng Cheng*, Jia-Jun Cai, Qing-Yan Zhou, Bing Liu, Zhen-Bo Wang*

Y. L. Zhang, Y. K. Dai, B. Liu, X. F. Gong, L. Zhao, J. J. Cai, Q. Y. Zhou, B. Liu, Z. B. Wang
MIIT Key Laboratory of Critical Materials Technology for New Energy Conversion and Storage, School of Chemistry and Chemical Engineering, State Key Lab of Urban Water Resource and Environment, Harbin Institute of Technology, No.92 West-Da Zhi Street, Harbin 150001, China.

F. Cheng
Key Laboratory for Advanced Technology in Environment Protection of Jiangsu Province, Yancheng Institute of Technology, Yancheng 224051, Jiangsu, China

This profile includes **Computational details, 18 Figures, 2 Table, 15 references.**

Experimental Section

Material Synthesis

Synthesis of CoCN: $Co(NO_3)_2·6H2O$ (0.06 g), $Zn(NO_3)_2·6H2O$ (0.53 g), and 2-methylimidazole (0.66 g) were dissolved in 30 mL of methanol to form solutions A and B, respectively. Then, they were mixed together and stirred for 1 hours and then let stand for another 24 h. After that, the solid powders could be collected after centrifugation and alcohol washing. Finally, the powders were carbonized at 900 °C for 3 h under 10% H_2/Ar atmosphere to gain the CoCN material. The synthesis method of CN is via the similar procedure except that no cobalt nitrate hexahydrate was introduced.

Synthesis of CoNi@CoCN： Firstly, two combustion boats of different sizes were prepared, the larger one was buckled over the smaller one, and a sheet of perforated carbon paper was sandwiched between them. 100 mg of nickelcene was placed in the combustion boat below, 50 mg of CoCN was placed on carbon paper, and then they were placed in a quartz tube in a PECVD apparatus. Afterwards, the pressure in the tube was drawn to 50 Pa, and then the temperature in the tube was raised to 120 ℃ and kept at 120 ℃ for 2 h. After allowed to cool naturally, the temperature was elevated to 700 ° C and maintained for 3 hours under a flow of 10% H_2/Ar. The synthesis method of Ni@CN is via the similar procedure except that CoCN was replaced by CN.

Characterization and Electrochemical test

Electron microscopy analysis was performed on the FEI Tecnai G2 F30 and NanoLab 600i. Nitrogen adsorption−desorption isotherm was collected by Quadrasorb Si analyzer. X-ray diffraction (XRD) experiments were characterized on a D/max-RB diffractometer. X-ray photoelectron spectroscopy (XPS) results were obtained on a Thermo Fisher ESCALAB 250Xi. The Raman measurements were obtained with Renishaw RM 1000 spectromicroscopy system.

Electrocatalytic activity tests

Electrocatalytic activity were tested on a CHI electrochemical analyzer. Ag/AgCl prefilled with KCl solution and a platinum mesh were employed the reference electrode and the counter electrode, respectively. The catalyst was dispersed on the mixed solution of ethanol and Nafion to form homogenous ink (5 mg mL^{-1}), whose volume ratio of the two liquid was 5:0.3. Then 20 uL ink was dropped onto the RRDE to form the working electrode. The electrochemical activity for ORR was determined using linear potential scan (LSV) with a potential step of 50 mV from 1.1 V to 0 V in O_2-saturated KOH. Stability of the catalysts were studied by consecutive 5000 cycles ranging from 0.6 V to 1 V and chronoamperometric responses at the potential of 0.7 V. The electrochemical activity for OER was determined by linear potential scan (LSV) with a potential step of 50 mV from 1.1 V to 1.7 V in 1 mol L^{-1} KOH. Stability of catalysts were studied by chronoamperometric responses at constant potential of 1.6 V.

Theoretical calculations

All calculations are carried out within the Density Generalized Function Theory (DFT) model, which is realized by the Vienna Abstract Simulation Package (VASP). We modeled the relationship between valence electrons and nuclei through the Projector Augmented Wave (PAW) potential database. In addition, the Perdew-Burke Ernzerh (PBE) and Generalized Gradient Approximation (GGA) of the exchange-correlation function were utilized to study the electron transfer situation. In the modeling process, we set the Gaussian smearing width to 0.1 eV, the unit lattice constant to 14.760 Å × 14.760 Å, and the vacuum layer to 30 Å. The conjugate gradient algorithm was employed to deal with the structural relaxation, limiting the maximum force and energy of unbound atoms to below 0.01 eV/Å and 1×10^{-6} eV, respectively. The electron iterative convergence value of the self-consistent field (SCF) calculation was similarly set to 1×10^{-6} eV.

Zn-air battery tests

CoNi@CoCN(2.5 mg), acetylene black (1 mg), XC-72 (4 mg), and Nafion diluent (8 μL) were dissolved by sonication in 300 ul of isopropanol to form a homogeneous ink. The air cathode was prepared and then placed in a vacuum drying oven. A polished zinc plate and 6 mol L^{-1} KOH aqueous solution with 0.2 mol L^{-1} $Zn(NO_3)_2$ were employed as the anode and electrolyte, respectively. Another set of Zn-battery with Pt/C+Ir/C, acetylene black and activated carbon as reference materials were used. The charge and discharge polarization curves were tested on CHI760E electrochemical workstation. The stability and cycling test of the Zn-air battery were determined with galvanostatically method on a Newware tester.

Table S1. Comparison of the bifunctional OER and ORR activity of CoNi@CoCN catalyst with other electrocatalysts previously reported.

Catalyst	$E_{1/2}$	E_{j10}	E_{j10}-$E_{1/2}$	Ref
Sulfur-doped carbon nanotube-graphene	0.79V	1.58V	0.79V	1
N-doped Carbon with topological defect	0.81V	1.75V	0.94V	2
Co-Ni alloy encapsulated by N-doped graphene	0.83V	1.63V	0.80V	3
Sulfurated CoNi MOF-derived Nanocomposites	0.79V	1.52V	0.73V	4
SAC of Co-N_4 on carbon substrates	0.88V	1.96V	1.08V	5
Atomically dispersed Fe via Ni neighboring	0.84V	1.69V	0.85V	6
Spinel $Co_xFe_{3-x}O_4$ nanoparticles	0.63V	1.71V	1.02V	7
Electronic and defective $CaMnO_3$ nanotubes	0.76V	1.70V	0.94V	8
Cation deficiency tuning of $LaCoO_3$ perovskite	0.65V	1.62V	0.97V	9
Layered double hydroxide/Mxene quantum dot metallic	0.68V	1.51V	0.83V	10
$NiCO_2O_4$ nanocrystal/Mxene hybrid	0.69V	1.55V	0.86V	11
Carbon nanosheets containing discrete Co-N_x-B_y-C	0.69V	1.70V	1.01V	12
Boron doped multi-walled carbon nanotubes	0.69V	1.81V	1.12V	13
Hybrid Co/Co–N–C Catalyst	0.85V	1.62V	0.77V	14
Tic-Modified A-MnO_2 Nanowires	0.72V	1.62V	0.91V	15
Pt/C+Ir/C	0.89V	1.60V	0.71V	
CoNi@CoCN catalyst	0.86 V	1.57V	0.71V	this work

Table S2. the adsorption free energy results of CoNi@CoCN, Co-N_4 with relevant O-containing intermediates

	G_{OH*} (eV)	G_{O*} (eV)	G_{OOH*} (eV)
CoNi@CoCN	1.1844	3.2663	4.1301
Co-N_4	0.6229	2.4688	3.75093

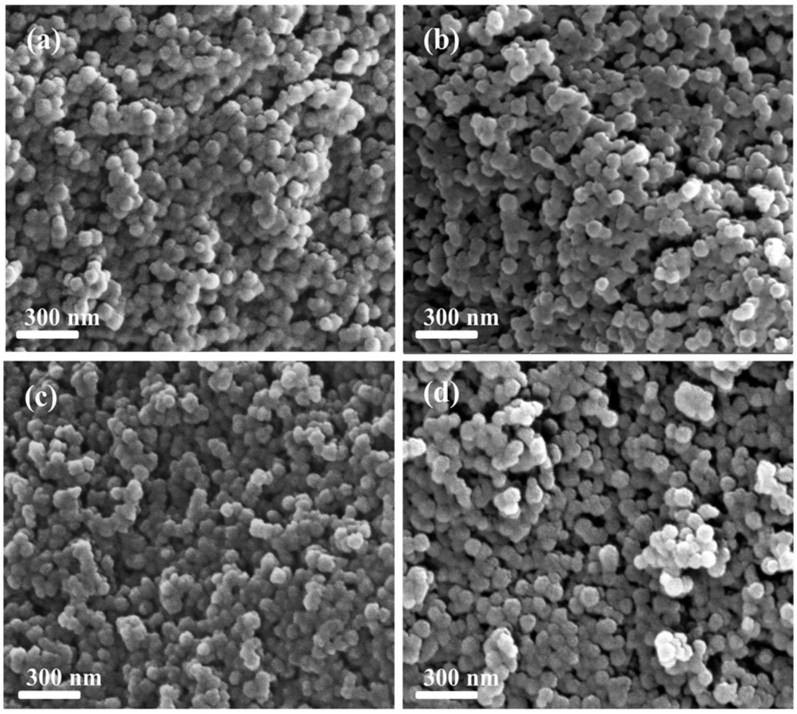

Figure S1 SEM images of (a) CN; (b) CoCN; (c) Ni@CN; (d) CoNi@CoCN.

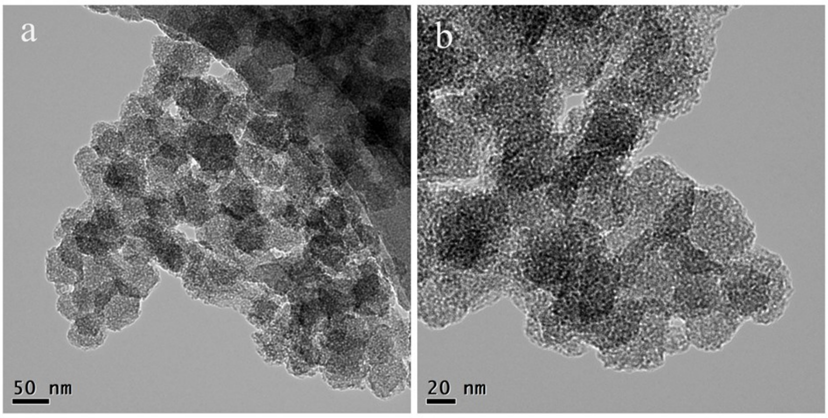

Figure S2. TEM images of CoCN

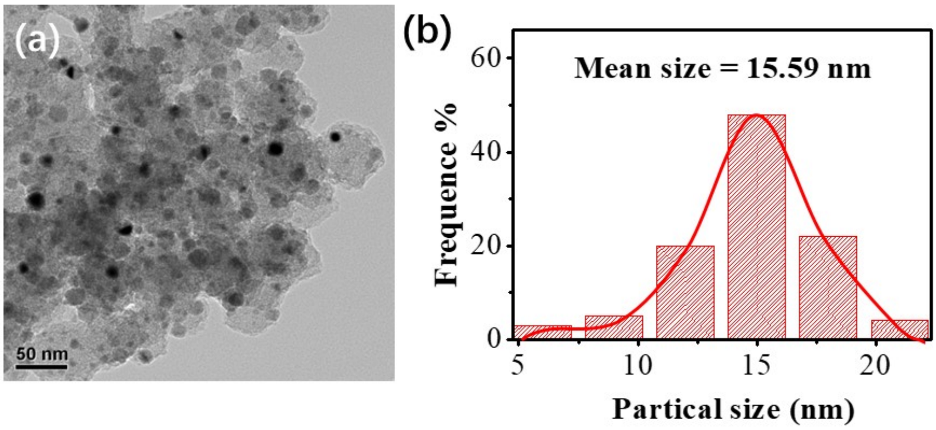

Figure S3 (a) TEM images and (b) size distribution of CoNi alloy nanoparticles of CoNi@CoCN.

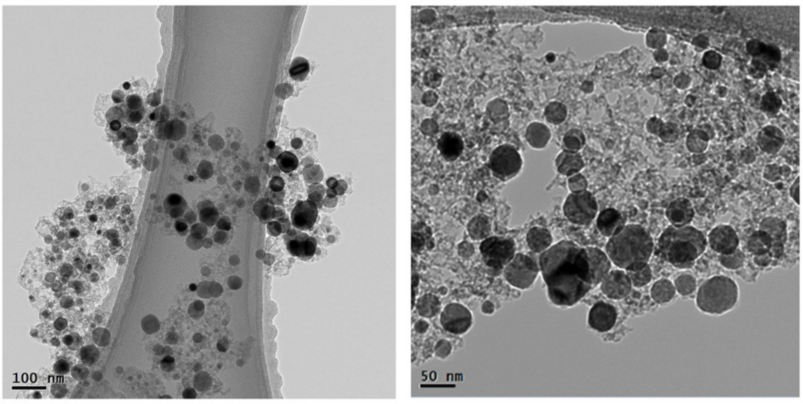

Figure S4 TEM images of CoNi@CoCN-WI.

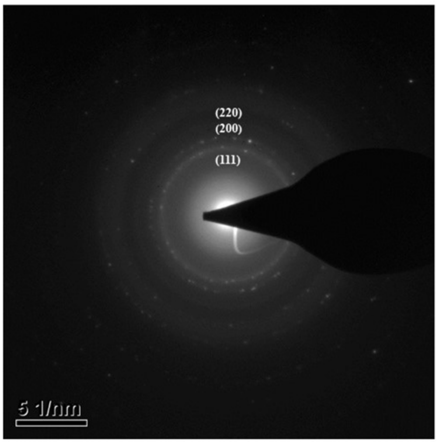

Figure S5 The diffraction ring in selected area electron diffraction of CoNi@CoCN.

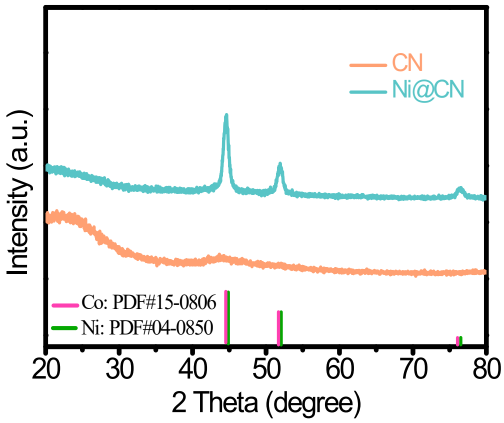

Figure S6 X-ray powder diffraction of Ni@CN and CN catalysts

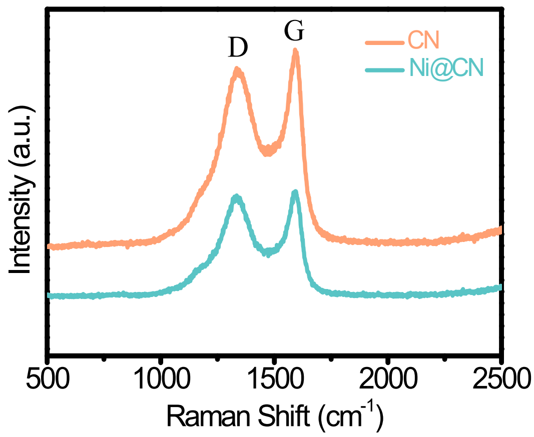

Figure S7 Raman measurements of Ni@CN and CN catalysts

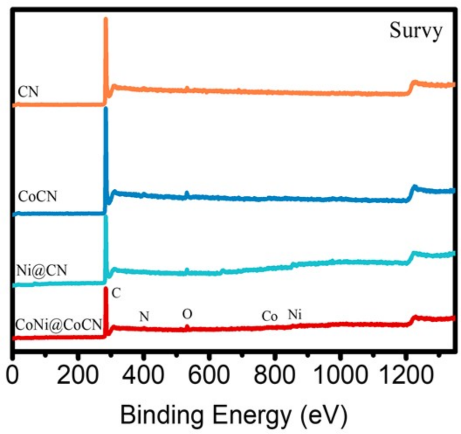

Figure S8 XPS spectra of the CoNi@CoCN catalysts and reference samples (CoCN, Ni@CN and CN catalysts).

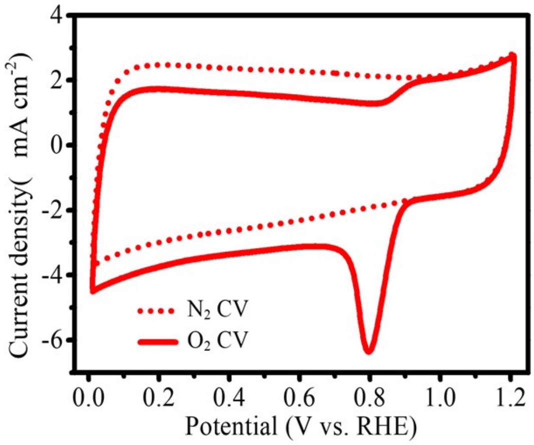

Figure S9 CV tests of CoNi@CoCN in O_2/N_2 saturated 0.1 mol/L KOH solution.

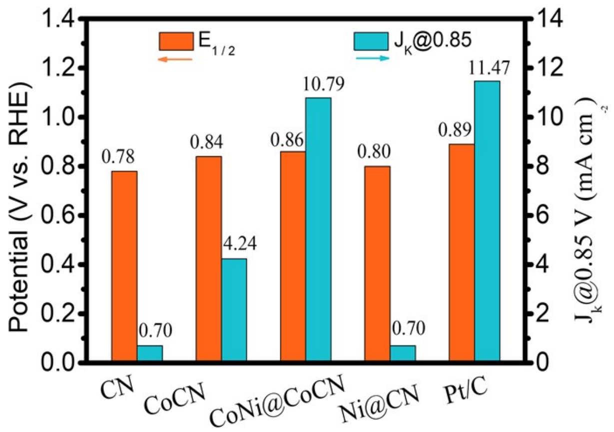

Figure S10 Bar plots of E_{onset} and $E_{1/2}$ for CoNi@CoCN catalyst and other comparison samples.

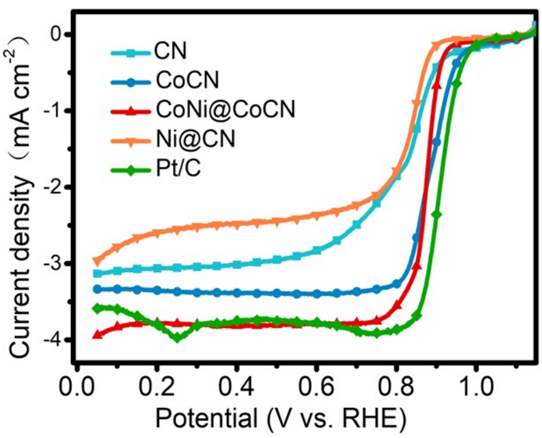

Figure S11 ORR polarization curves of CoNi@CoCN, CoCN, Ni@CN, CN, and Pt/C in 1M KOH solution.

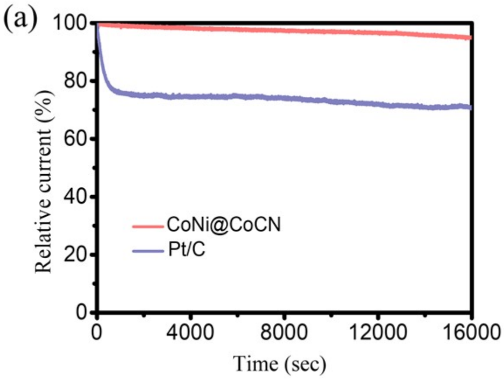

Figure S12 (a) Chronoamperometric measurement of ORR for CoNi@CoCN and Pt/C, (b) LSV curve of Pt/C before and after aging.

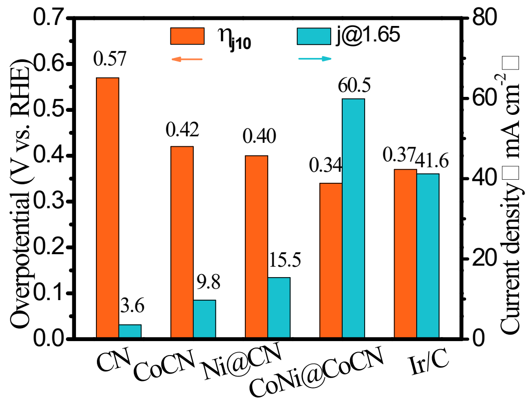

Figure S13 Bar plots of η_{j10} and j@1.65 V for CoNi@CoCN catalyst and other comparison samples.

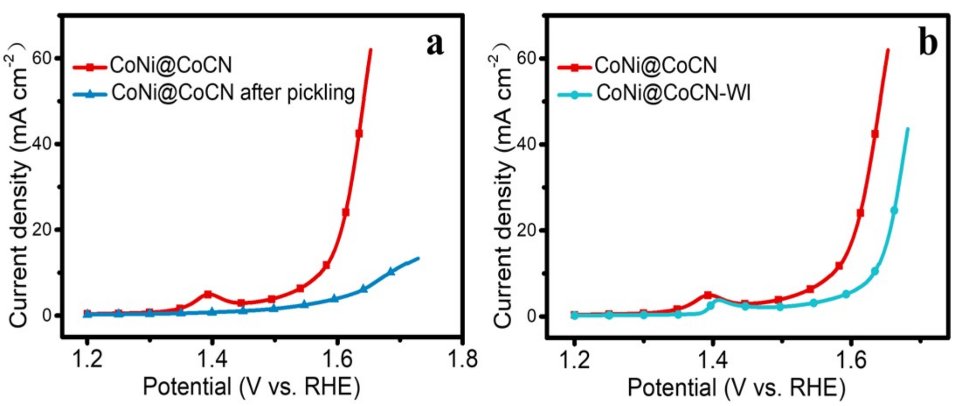

Figure S14 OER polarization curves of CoNi@CoCN, CoNi@CoCN catalyst after pickling, and CoNi@CoCN-WI in 1M KOH solution.

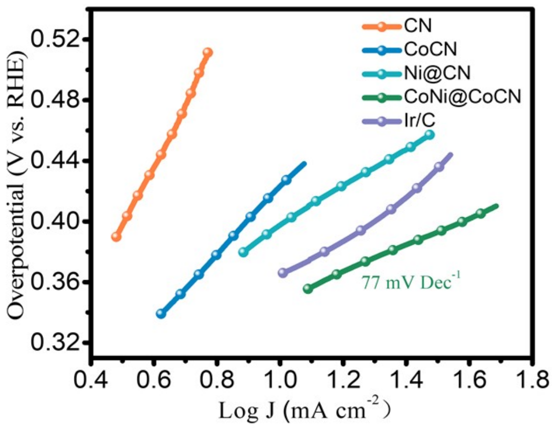

Figure S15 Tafel plots of five catalysts for OER.

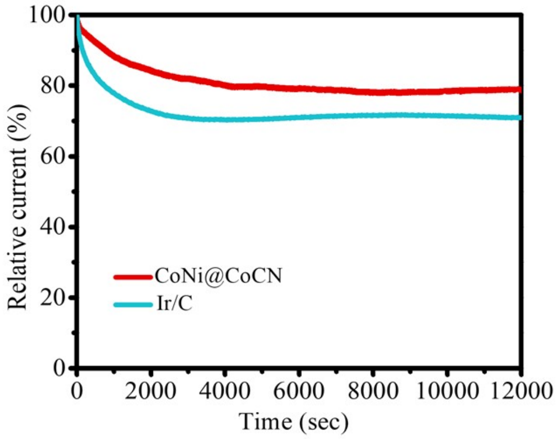

Figure S16 Chronoamperometric measurement of OER for CoNi@CoCN and Ir/C.

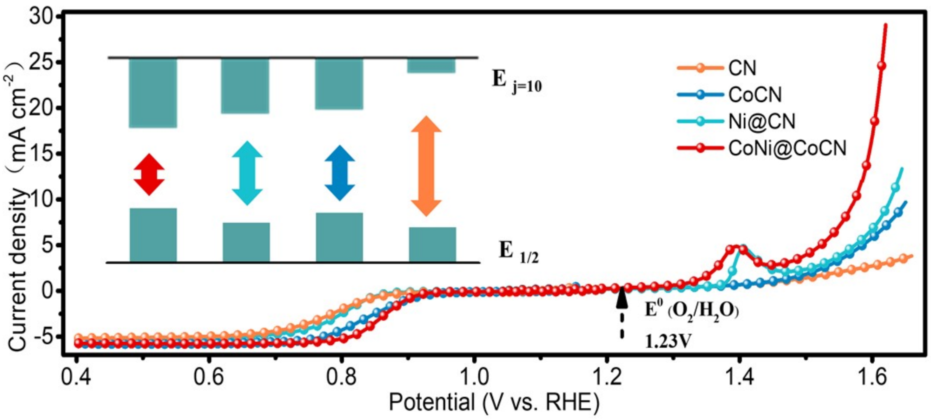

Figure S17 The overall polarization curves of catalysts within the ORR and OER potential window; inset shows the value of ΔE for catalysts ($\Delta E = E_{j10} - E_{1/2}$).

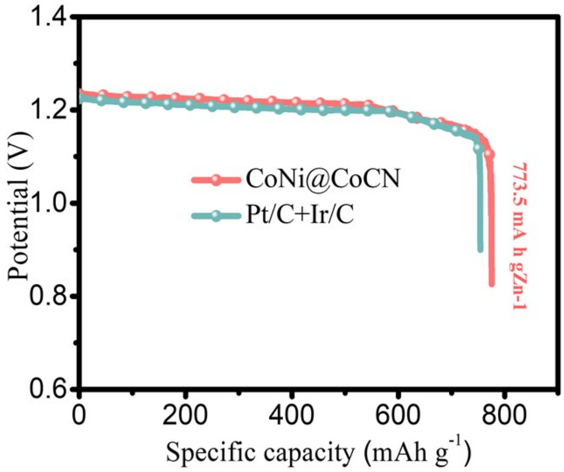

Figure S18 The specific capacity results at a constant current density of CoNi@CoCN and Pt/C+Ir/C.

References

[1] A. M. El-Sawy, I. M. Mosa, D. Su, C. J. Guild, S. Khalid and R. Joesten, *Adv. Energy Mater.*, 2016, **6**, 1501966.

[2] Y. Y. Liu, K. Sun, X. Y. Cui, B. J. Li and J. C. Jiang, *ACS Sustainable Chem. Eng*., 2020, **8**, 2981–2989.

[3] Z. Chang, F. Yu, Z. Liu, S. Peng, M. Guan and X. Shen, *ACS Appl. Mater. Interfaces*, 2020, **12**, 4366–4372.

[4] Z. Wu, H. Wu, T. Niu, S. Wang, G. Fu, W. Jin and T. Ma, *ACS Sustainable Chem. Eng*., 2020, **8**, 9226–9234.

[5] K. Kim, T. Kang, M. Kim, and J. Kim, *Appl. Catal. B*, 2020, **275**, 119107.

[6] M. Ma, A. Kumar, D. Wang, Y. Wang and Y. Jia, Y. Zhang, *Appl. Catal. B*, 2020, **274**, 119091.

[7] Q. Wang, Y. Xue, S. Sun, S. Yan, H. Miao and Z. Liu, *J. Power Sources*, 2019, **435**, 226761.

[8] S. Peng, X. Han, L. Li, S. Chou, D. Ji and H. Huang, *Adv. Energy Mater.*, 2018, **8**, 1800612.

[9] H. Luo, H. Wang, X. Chen, D. Huang and D. Ding, *ChemCatChem*, 2020, **12**, 2768–2775.

[10] X. Han, N. Li, P. Xiong, G.J. Min and H.S. Park, *Infomat*, 2021, 1-11.

[11] H. Lei, S. Tan, L. Ma, Y. Liu, Y. Liang and M.S. Javed, *ACS Appl.* Mater. Interfaces, 2020, **12**, 44639-44647.

[12] Y. Guo, P. Yuan, J. Zhang, Y. Hu, I.S. Amiinu and X. Wang, *ACS Nano*, 2018, **12**, 1894-1901.

[13] Y. Cheng, Y. Tian, X. Fan, J. Liu and C. Yan, *Electrochimic. Acta*, 2014, **143**, 291-296.

[14] D. Wang, P. Yang, H. Xu, J. Ma, L. Du and G. Zhang, *J. Power Sources*, 2021, **485**, 229339.

[15] S. Song, W. Li, Y. Ruan, X. Qin, D. Zhang and Y. Xu, *J. Alloys Compd*., 2020, **834**, 155090.